Spin Nernst effect and Nernst effect in two-dimensional electron systems

Shu-guang Cheng[1], Yanxia Xing[1], Qing-feng Sun[1,*], and X. C. Xie[2,1]
[1]*Institute of Physics, Chinese Academy of Sciences, Beijing 100190, China*
[2]*Department of Physics, Oklahoma State University, Stillwater, Oklahoma 74078*

We study the Nernst effect and the spin Nernst effect, that a longitudinal thermal gradient induces a transverse voltage and a spin current. A mesoscopic four-terminal cross-bar device having the Rashba spin-orbit interaction (SOI) under a perpendicular magnetic field is considered. For zero SOI, the Nernst coefficient peaks when the Fermi level crosses the Landau Levels. In the presence of the SOI, the Nernst peaks split, and the spin Nernst effect appears and exhibits a series of oscillatory structures. The larger SOI is or the weaker magnetic field is, the more pronounced the spin Nernst effect is. The results also show that the Nernst and spin Nernst coefficients are sensitive to the detailed characteristics of the sample and the contacts. In addition, the Nernst effect is found to survive in strong disorder than the spin Nernst effect does.

PACS numbers: 72.15.Jf, 72.25.-b, 73.23.-b, 73.43.-f

The Hall-like effect, namely, a longitudinal force induces a transverse current, has been a fascinating topic since the early days of the condensed matter physics. The integer and the fractional quantized Hall effects, two celebrating examples, have been extensively investigated for the last three decades, but remain to be active research fields till now. Recently, another Hall-like effect, spin Hall effect, in which a longitudinal voltage bias induces a transverse spin current due to the scattering by magnetic impurities or due to the existence of a spin-orbit interaction (SOI), has generated a great deal of interest.[1,2] Apart from a large number of theoretical studies, several experimental investigations also made important contributions to the field. Up to now, SOI has indeed been found to be substantial in some semiconductors despite it is a relativistic effect, and its strength can be tuned by the gate voltage in the experiment.[3,4] In particular, the spin Hall effect has been detected experimentally by observing the transverse opposite-spin accumulations near the two edges of the sample.[5,6]

The Nernst effect, a thermoelectric property, in which a longitudinal thermal gradient induces a transverse current (or a bias ΔV with open boundary) while under a perpendicular magnetic field, is also a Hall-like effect. The thermoelectric coefficients (including the Seebeck coefficient and the Nernst coefficient) of electronic systems are known to be more sensitive to the details of the density of states than the conductance,[7,8,9] and these detailed information of the density of states is importance for the design of the electronic devices. But the thermoelectric measurement is usually more difficult to carry out than the conventional transport measurements, particularly for low-dimensional systems or nano-devices. Fortunately, because of the development of the microfabrication technology and the low-temperature measurement technology in the last two decades, the thermoelectric measurement in low-dimensional samples has been feasible now.[10,11] Recently, the thermopower of the quantum dot was measured, and the results in the Kondo regime show a clear deviation from the semiclassical Mott relation.[10,12] The Nernst effect in bismuth has also been detected and the Nernst coefficient peaks at positions when Fermi level crosses over the Landau levels (LLs).[13] Meanwhile, limited theoretical studies of the Nernst effect have also appeared.[14]

In this paper, we study the Nernst effect and spin Nernst effect in a two-dimensional electron gas with a SOI and under a perpendicular magnetic field B. For the first time, the spin Nernst effect, a novel Hall-like effect, is investigated. The spin Nernest effect implies that a longitudinal thermal gradient $\Delta\mathcal{T}$ induces a transverse spin current. The spin Nernst coefficient should be more sensitive to the details of the spin density of states of the system than the spin Hall conductance, similar as their electronic counterparts.[7,8,9] We consider the system as shown in Fig.1a, consisting of a square center region connected to four ideal semi-infinite leads. A longitudinal thermal gradient $\Delta\mathcal{T}$ is added between the leads 1 and 3. This thermal gradient induces a transverse Hall voltage V_H with the open boundary condition under a perpendicular magnetic field B; a transverse spin current J_{sH} in the closed boundary condition with a SOI. By using a tight-binding model and the Landauar-Buttiker (LB) formula with the aid of the Green's functions, the Nernst coefficient N_e ($N_e \equiv V_H/\Delta\mathcal{T}$) and spin Nernst coefficient N_s ($N_s \equiv J_{sH}/\Delta\mathcal{T}$) are calculated. Without a SOI, the Nernst coefficient N_e peaks when the Fermi level E_F crosses the LLs, and spin Nernst coefficient N_s is absent, consistent with the recent experimental findings.[13] In the presence of a SOI, each LL splits into two, consequently, each Nernst peak splits into two peaks. Meanwhile, the spin Nernst effect emerges and its coefficient N_s exhibits a series of oscillatory structures. The oscillation is enhanced with increasing SOI but is damped by a large B. In addition, the Nernst effect is found to survive in strong disorder than the spin Nernst effect does.

In the tight-binding representation, the cross-bar sample is described by the Hamiltonian:[15],

$$H = -t\sum_{\mathbf{i}\sigma}[c^{\dagger}_{\mathbf{i}+\delta x,\sigma}c_{\mathbf{i}\sigma}e^{-im\theta} + c^{\dagger}_{\mathbf{i}+\delta y,\sigma}c_{\mathbf{i}\sigma} + H.c.]$$

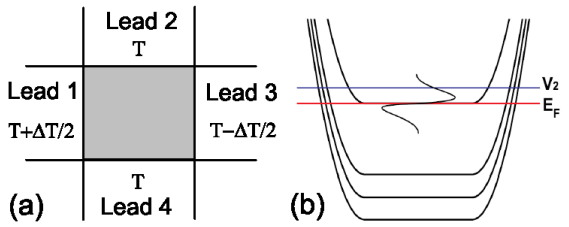

FIG. 1: (color online) (a) Schematic diagram for the four-terminal cross-bar sample with a thermal gradient $\Delta\mathcal{T}$ applied between the longitudinal lead-1 and lead-3. (b) Schematic view of the LLs of the center region, the Fermi energy E_F, and the bias V_2. The oscillatory line across E_F is the difference of $f_1(E) - f_2(E)$.

$$+ \sum_{\mathbf{i}\sigma} \varepsilon_{\mathbf{i}} c^\dagger_{\mathbf{i}\sigma} c_{\mathbf{i}\sigma} - V_R \sum_{\mathbf{i}\sigma\sigma'} [c^\dagger_{\mathbf{i}+\delta y,\sigma} (i\sigma_x)_{\sigma\sigma'} c_{\mathbf{i}\sigma'} - c^\dagger_{\mathbf{i}+\delta x,\sigma} (i\sigma_y)_{\sigma\sigma'} c_{\mathbf{i}\sigma'} e^{-im\theta} + H.c.] \quad (1)$$

where $c^\dagger_{\mathbf{i}\sigma}(c_{\mathbf{i}\sigma})$ is the creation (annihilation) operator of electrons in the site $\mathbf{i} = (n, m)$ with spin σ. $t = \hbar^2/(2m^*a^2)$ is the hopping matrix element with the lattice constant a, and δx and δy are the unit vectors along the x and y directions. $\varepsilon_{\mathbf{i}}$ is the on-site energy, which is set to 0 everywhere for the clean system. While in a disorder system, $\varepsilon_{\mathbf{i}}$ in the center region is set by a uniform random distribution [-W/2,W/2]. The last term in Eq.(1) represents the Rashba SOI with V_R being its strength. In order to avoid confusion in calculating the spin current, V_R is set to zero in the lead-2 and lead-4. The extra phase $\theta = ea^2B/h$ is from the perpendicular magnetic field B. Here the Zeeman effect and electron-electron interaction are neglected.[16] The Zeeman split could be small in some of the two-dimensional electron systems. The electron-electron interaction is weak in systems with high carrier density.

The particle current $J_{p\sigma}$ in the transverse lead-p with spin $\sigma =\uparrow, \downarrow$ can be obtained by the LB formula:[15]

$$J_{p\sigma} = \frac{1}{\hbar} \sum_{q\neq p} \int dE\ T_{p\sigma,q}(E)[f_p(E) - f_q(E)] \quad (2)$$

where $T_{p\sigma,q}(E)$ is the transmission coefficient from the lead-q to the lead-p with spin σ and E is the energy of the incident electron. The transmission coefficient can be calculated from: $T_{p\sigma,q}(E) = Tr[\mathbf{\Gamma}_{p\sigma}\mathbf{G}^r\mathbf{\Gamma}_q\mathbf{G}^a]$, where the line-width function $\mathbf{\Gamma}_{p\sigma}(E) = i(\mathbf{\Sigma}^r_{p\sigma} - \mathbf{\Sigma}^{r\dagger}_{p\sigma})$, $\mathbf{\Gamma}_q = \mathbf{\Gamma}_{q\uparrow} + \mathbf{\Gamma}_{q\downarrow}$, and $\mathbf{\Sigma}^r_{p\sigma}$ is the retarded self-energy due to coupling to the lead-p with spin σ. The Green's function $\mathbf{G}^r(E) = [\mathbf{G}^a(E)]^\dagger = \{E\mathbf{I} - \mathbf{H}_0 - \sum_{p\sigma} \mathbf{\Sigma}^r_{p\sigma}\}^{-1}$ and $\mathbf{H}_0$ is the Hamiltonian of the central region. $f_p(E)$ in Eq.(2) is the electronic Fermi distribution function of the lead-p, and $f_p(E) = 1/\{\exp[(E - E_F - V_p)/k_B\mathcal{T}_p] + 1\}$ with the bias V_p and temperature $\mathcal{T}_p$. After getting the particle current $J_{p\sigma}$, the (charge) current is $J_{pe} = e(J_{p\uparrow} + J_{p\downarrow})$ and the spin current is $J_{ps} = (\hbar/2)(J_{p\uparrow} - J_{p\downarrow})$.

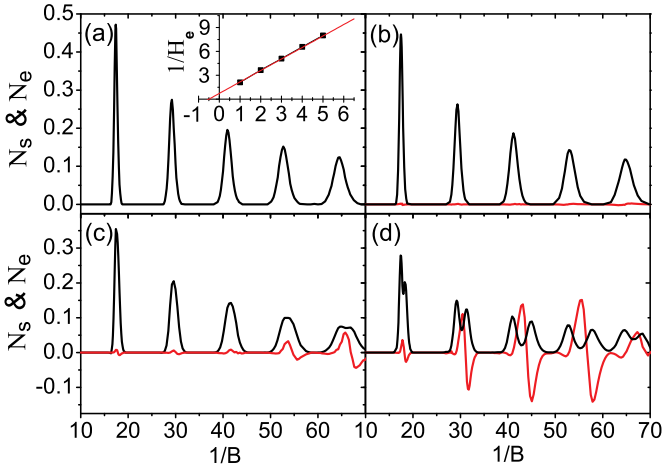

FIG. 2: (color online) N_e (black) and N_s (red or gray) vs. $1/B$ for different $V_R = 0$ (a), 0.02 (b), 0.05 (c), and 0.1 (d). The other parameters are $E_F = -3$, the size of the center region $L = 40a$, and $\mathcal{T} = 0.01$. In the inset of (a), the dots are the inverse of peaks' maxima vs. Nth peak, and the line is $(N + \frac{1}{2})/\ln 2$ vs. N.

Considering a small temperature gradient $\Delta\mathcal{T}$ and zero bias applied on the longitudinal lead-1,3, we can set the temperatures $\mathcal{T}_1 = \mathcal{T} + \Delta\mathcal{T}/2$, $\mathcal{T}_3 = \mathcal{T} - \Delta\mathcal{T}/2$, $\mathcal{T}_2 = \mathcal{T}_4 = \mathcal{T}$, and the biases $V_1 = V_3 = 0$. From the open boundary condition with $J_{2e} = J_{4e} = 0$, the transverse voltage V_2 and V_4 can be obtained, and consequently the Nernst coefficient $N_e = (V_2 - V_4)/\Delta\mathcal{T}$. In the clean system, N_e is expressed as

$$N_e = \frac{1}{e\mathcal{T}} \frac{\int dE\ (T_{21} - T_{23})(E - E_F)f(1-f)}{\int dE\ (T_{21} + T_{23} + 2T_{24})f(1-f)}, \quad (3)$$

where $T_{2p} = T_{2\uparrow,p} + T_{2\downarrow,p}$. The spin Hall current J_{2s} and J_{4s} are calculated with the closed boundary condition having $V_2 = V_4 = 0$. In the clean system, $J_{2s} = -J_{4s}$ because of the symmetry property of the system. In a dirty system, J_{2s} may not equal to $-J_{4s}$ for a given disorder configuration, but $J_{2s} = -J_{4s}$ still holds after average over many configurations. The spin Nernst coefficient $N_s \equiv J_{2s}/\Delta\mathcal{T}$, and can be reduced to:

$$N_s = \frac{1}{4\pi} \int dE(\Delta T_{23} - \Delta T_{21}) \frac{E - E_F}{k_B\mathcal{T}^2} f(1-f), \quad (4)$$

where $\Delta T_{2p} = T_{2\uparrow,p} - T_{2\downarrow,p}$. At low temperature limit ($\mathcal{T} \to 0$), the Nernst coefficient N_e and the spin Nernst coefficient N_s usually depend linearly on temperature. But while $\frac{\partial E}{\partial(T_{21}-T_{23})}|_{E=E_F} = 0$ ($\frac{\partial E}{\partial(\Delta T_{21}-\Delta T_{23})}|_{E=E_F} = 0$), or in other words $T_{21} - T_{23}$ ($\Delta T_{21} - \Delta T_{23}$) at $E = E_F$ is discontinuous, N_e (N_s) is temperature independent.

In the numerical calculations, we set $t = \hbar^2/(2m^*a^2)$ as the energy unit and $\frac{e}{h}a^2$ as the unit of the magnetic field B. If taking the effective electron mass

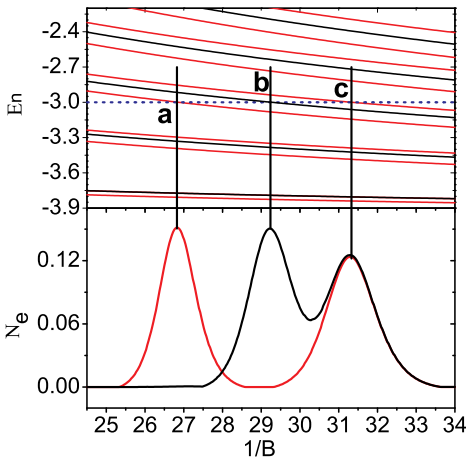

FIG. 3: (color online) (up panel) The LLs E_n vs. $1/B$ for $V_R = 0$ (black) and 0.1 (red or gray). The blue dotted line is the Fermi level E_F. (down panel) N_e vs. $1/B$ for the Rashba SOI in lead-2, 4 is 0 (black) and 0.1 (red or gray). The parameters are $E_F = 1.0$, $V_R = 0.1$, $L = 20a$, and $\mathcal{T} = 0.01$.

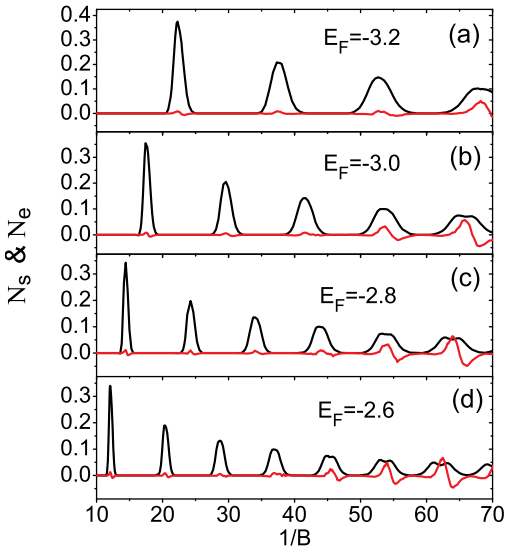

FIG. 4: (color online) N_e (black) and N_s (red or gray) vs. $1/B$ for different Fermi level E_F with the parameters $V_R = 0.05$, $\mathcal{T} = 0.01$, and $L = 40a$.

$m^* = 0.05m_e$ and the lattice constant $a = 12.5nm$, t is about $5meV$, $B = 1$ corresponds to 4.2 Tesla, and $V_R = 0.1t$ corresponds to the Rashba SOI parameter $\alpha = 1.25\times10^{-11}$eV·m which can be experimentally modulated by the gate voltage. We consider square samples and the center-region size is either $L = 40a$ or $L = 20a$ in our calculations. Temperature is fixed at $\mathcal{T} = 0.01$, that is about $1K$.

Fig.2 shows the Nernst coefficient N_e and spin Nernst coefficient N_s versus the inverse of magnetic field $1/B$ for the different SOI strength V_R in the clean system ($W = 0$). While without the SOI ($V_R = 0$), N_s is exactly zero, but N_e exhibits a series of equal spacing peaks. N_e peaks when the Fermi level E_F crosses over LLs, and it is damped when E_F lies between adjacent LLs. The peak interval is $e\hbar/(m^*E_F^*)$ where $E_F^* = E_F + 4t$ is the distance from the Fermi energy to the band bottom $-4t$. The inverse of the height H_e of the Nth peak is linearly dependent on N, with $H_e \propto N + 1/2$ (as shown in inset of Fig.2a). Let us explain these characteristics with aids of the physical picture in Fig.1b. Under a strong B, the transmission coefficients $T_{23}(E)$ and $T_{24}(E)$ are usually zero, and $T_{21}(E)$ is an integer. Then the current $J_{2e} = (e/h)\int dE T_{21}(E)[f_2(E) - f_1(E)]$ from Eq.(2). Due to the thermal gradient, $f_2 - f_1$ exhibits an oscillatory structure around E_F as shown in Fig.1b, and the electrons with energy above and below E_F contribute opposite signs to the thermocurrent J_{2e}. When all LLs are far from E_F, T_{21} is a constant near E_F, the currents flowing in or out cancel each other, leading to $J_{2e} = 0$ at $V_2 = 0$. On the other hand, when N LLs are below E_F but one LL is at E_F (see Fig.1b), a net current J_{2e} is induced at $V_2 = 0$. In the open circuit case, V_2 has to be raised to make $J_{2e} = 0$, and V_2 is the ratio $1/(2N + 1)$. In fact, from Eq.(2) and assuming that $T_{32} = T_{42} = 0$ and T_{21} is an integer for large B, we can analytically obtain that the peak height of the Nernst coefficient is $H_e = \frac{k_B}{e} ln2/(N + 1/2)$. This result is identical with the result of the thermopower in a two-terminal system.[17]

While in the presence of a SOI ($V_R \neq 0$), the LLs split. As a result, the peaks of the Nernst coefficient N_e also split and the spin Nernst coefficient N_s emerges (see Fig.2). The splitting is more pronounced for stronger SOI V_R or weaker magnetic field B. The positions of the right sub-peaks of N_e are consistent with LLs, but not the left sub-peaks. To see this, we magnify the second peak of Fig.2d, and also plot in Fig.3 the LLs versus $1/B$ without SOI ($V_R = 0$) and with SOI ($V_R \neq 0$). It clearly shows that the left sub-peak is in line with the original un-split LL at $V_R = 0$ (see mark b in Fig.3), not in alignment with the split LLs. In order to thoroughly study the peak positions, we also plot N_e for the uniform system, in which SOI exists in all parts, including the leads-2, 4. Now the left sub-peak moves to align with the split LL. (see mark a in Fig.3). So the counterintuitive phenomena entirely comes from the non-uniformity of SOI, in which the SOI is absent in the leads-2, 4 and an interface between $V_R = 0$ and $V_R \neq 0$ emerges. This interface causes additional scattering for an incident electron, and one of the edge states goes directly from lead-1 to lead-3 instead of from lead-1 to lead-2, so the left sub-peak position in N_e is moved. This means that the Nernst effect can reflect the detailed structure of the transverse leads and its contact to the sample. This is essential difference to the regular Hall effect.[7,8,9]

Next, we study the spin Nernst coefficient N_s, which emerges with $V_R \neq 0$ (see Fig.2b-d). In the vicinity of the right sub-peak of N_e, N_s exhibits an oscillatory structure

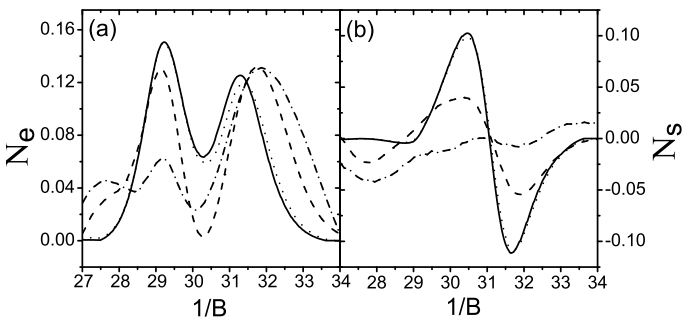

FIG. 5: N_e (a) and N_s (b) vs. $1/B$ for the different disorder strengths $W = 0$ (solid curve), 0.1 (dotted curve), 0.5 (dashed curve), and 1.0 (dash-dotted curve). The other parameters are $E_F = -3$, $V_R = 0.1$, $\mathcal{T} = 0.01$, and $L = 20a$.

and $N_s \propto \partial[lnN_e(E_F)]/\partial E_F$. This relation of N_s and N_e is similar to the semiclassical Mott relation between the thermopower and conductance.[17] However, N_s is quite small and does not show an oscillatory structure around the left sub-peak of N_e, and the Mott-like relation breaks there. We can qualitatively analyze these phenomena using Schrödinger equation, in which we can analytically obtain the split LLs and corresponding wave functions. It is found that for weak SOI (such as $V_R < 0.1t$), the wave functions of the high sub-LLs are strongly spin polarized in the z-direction, while one of the low sub-LLs are hardly spin polarized. As a result, the spin current $J_{2,4s}$ with an oscillatory structure only exists when E_F crosses over the high sub-LLs, which corresponds to the positions of the right sub-peaks of N_e. In addition, a larger SOI or a weaker magnetic field will cause a stronger spin Nernst signals (see Fig.2), due to the competition between the magnetic field and the SOI. In fact, the Rashba SOI is to drive the electrons with opposite spins to opposite directions transversely which leads to the spin Nernst effect, but a magnetic field B is to drive all electrons in the same transverse direction. Thus, B weakens the spin Nernst effect.

The relation of the LLs E_N with the magnetic field B is: $E_N = \frac{eB\hbar}{m^*}(N + 1/2) - 4t$, so the period in the Nernst signal is $e\hbar/(m^* E_F^*)$, changeable by adjusting the Fermi level E_F. In Fig.4, we plot N_e and N_s as functions of the inverse of B for different E_F. The results for different E_F show similar behaviors. With increasing of E_F, the peaks of N_e and the oscillatory structures of N_s are getting closer, and the magnitudes of N_e and N_s signals at same filling factors are getting weaker.

Finally we discuss the disorder effect on the Nernst and spin Nernst effects. Fig.5 shows N_e and N_s versus the inverse B for different disorder strength W. Here N_e and N_s are averaged over 500 disorder configurations. For a small disorder (e.g. $W = 0.1$), both N_e and N_s are hardly affected. For an intermediate disorder, such as $W = 0.5$, the two sub-peak heights of N_e almost keep their strengths as for $W = 0$, but the valley between two sub-peaks is greatly deepened, so that the two sub-peak structure is even clearer (see Fig.5a). With further increasing of the disorder W, the left sub-peak of N_e is decreased while the right sub-peak is less affected, meanwhile the oscillatory structure of N_s is weakened. However, in the vicinity of the left sub-peak of N_e, the spin Nernst coefficient N_s, which is very small at $W = 0$, is enhanced by W (see Fig.5b). Finally, for very large disorder W, the system goes into an insulating regime, both N_e and N_s vanish.

Before summary, we would like to make a couple comments concerning the novel spin Nernst effect. (i) The spin Nernst effect is NOT a simple combination of the Seebeck effect and the spin Hall effect. In fact, the Seebeck coefficient is mainly determined by $(dT_{13}(E))/(dE)|_{E=E_F}$, while the spin Nernst coefficient depends on ΔT_{23} and ΔT_{21}. (ii) The spin Nernst effect can be measured in similar ways that the spin Hall effect is observed,[5,6] e.g. through spin accumulations.

In summary, the Nernst effect and spin Nernst effect in a two-dimensional cross-bar with a spin-orbit interaction and under a perpendicular magnetic field are investigated. The Nernst signal exhibits a series of peaks, and the inverse of a peak height goes linearly to the sequence number of the peak. While in the presence of a SOI, these Nernst peaks split, and the spin Nernst effect appears, which exhibits an oscillatory structure versus the magnetic field. The relation of the Nernst and spin Nernst coefficients is similar to the semiclassical Mott relation around one sub-peak, but has a great discrepancy around the other sub-peak. In addition, the disorder effect on the Nernst and spin Nernst effects is also discussed.

Acknowledgments: We gratefully acknowledge the financial support from the Chinese Academy of Sciences, US-DOE under Grant No. DE-FG02-04ER46124 and US-NSF, and NSF-China under Grant Nos. 10525418, 60776060, and 10734110.

* Electronic address: sunqf@aphy.iphy.ac.cn

[1] J. E. Hirsch, Phys. Rev. Lett. **83**, 1834 (1999); M. I. Dyakonov and V. I. Perel, JETP Lett. **13**, 467 (1971); Phys. Lett. A **35**, 459 (1971).

[2] S. Murakami, N. Nagaosa, and S.C. Zhang, Science **301**, 1348 (2003); J. Sinova, D. Culcer, Q. Niu, N. A. Sinitsyn, T. Jungwirth, and A. H. MacDonald, Phys. Rev. Lett. **92**, 126603 (2004).

[3] J. Nitta, T. Akazaki, H. Takayanagi, and T. Enoki, Phys. Rev. Lett. **78**, 1335 (1997); T. Bergsten, T. Kobayashi, Y. Sekine, and J. Nitta, Phys. Rev. Lett. **97**, 196803 (2006).

[4] J. P. Heida, B. J. van Wees, J. J. Kuipers, T. M. Klapwijk, and G. Borghs, Phys. Rev. B **57**, 11911 (1998); D. Grundler, Phys. Rev. Lett. **84**, 6074 (2000).

[5] Y. K. Kato, R. C. Myers, A. C. Gossard, and D. D. Awschalom, Science **306**, 1910 (2004); J. Wunderlich, B. Kaestner, J. Sinova, and T. Jungwirth, Phys. Rev. Lett. **94**, 047204 (2005); V. Sih, R. C. Myers, Y. K. Kato, W. H. Lau, A. C. Gossard, and D. D. Awschalom, Nature Phys. **1**, 31 (2005); V. Sih, W. H. Lau, R. C. Myers, V. R. Horowitz, A. C. Gossard, and D. D. Awschalom, Phys. Rev. Lett. **97**, 096605 (2006).

[6] S. O. Valenzuela and M. Tinkham, Nature (London) **442**, 176 (2006).

[7] A.A. Abrikosov, *Fundamentals of the theory of metals* (NorthHolland Amsterdam, 1988).

[8] J.M. Iiman, *Electrons and phonons* (Oxford university Press, Oxford, U.K., 1960).

[9] C.W.J. Beenakker and A.A.M. Staring, Phys. Rev. B **46**, 9667 (1992).

[10] A. S. Dzurak, C. G. Smith, C. H. W. Barnes, M. Pepper, L. Martin-Moreno, C. T. Liang, D. A. Ritchie, and G. A. C. Jones, Phys. Rev. B **55**, R10197 (1997); R. Scheibner, H. Buhmann, D. Reuter, M. N. Kiselev, and L. W. Molenkamp, Phys. Rev. Lett. **95**, 176602 (2005); R. Scheibner, E. G. Novik, T. Borzenko, M. K*ö*nig, D. Reuter, A. D. Wieck, H. Buhmann, and L. W. Molenkamp, Phys. Rev. B **75**, R041301 (2007).

[11] L. W. Molenkamp, H. van Houten, C. W. J. Beenakker, R. Eppenga, and C.T. Foxon, Phys. Rev. Lett. **65**, 1052 (1990).

[12] M. Cutler and N. F. Mott, Phys. Rev. **181** 1336, (1969).

[13] K. Behnia, M.-A. M*é*asson, and Y. Kopelevich, Phys. Rev. Lett. **98**, 166602 (2007); K. Behnia, L. Balicas, and Y. Kopelevich, Science **317**, 1729 (2007).

[14] H. Nakamura, N. Hatano, and R. Shirasaki, Solid State Communications **135**, 510 (2005); R. Shirasaki, H. Nakamura, N. Hatano, J. Surf. Sci. Nanotech. Vol. **3**, 518 (2005).

[15] L. Sheng, D. N. Sheng, and C. S. Ting, Phys. Rev. Lett. **94**, 016602 (2005); W. Ren, Z. Qiao, J. Wang, Q. Sun, and H. Guo, Phys. Rev. Lett. **97**, 066603 (2006); Z. Qiao, W. Ren, J. Wang, and H. Guo, Phys. Rev. Lett. **98**, 196402 (2007); Y. Xing, Q.-F. Sun, and J. Wang, Phys. Rev. B **75**, 075324 (2007).

[16] If the Zeeman effect is included, the Nernst peaks in Fig.2 are split and the spin Nernst effect is induced. Then two kinds of oscillatory structures respectively from the Zeeman effect and Rashba SOI appear in the spin Nernst coefficient N_s. This behavior is similar as in the spin Hall effect, in which two kinds of peaks also appear. See Y. Xing, Q.-F. Sun, and J. Wang, Phys. Rev. B **77**, 115346 (2008) for detail.

[17] P. Streda, J. Phys.: Condens. Matter **1** 1025 (1989).